Channel-coupling effects in the resonating-group study of the seven-nucleon system

Y. Fujiwara and Y. C. Tang

School of Physics, University of Minnesota, Minneapolis, Minnesota 55455

(Received 7 June 1983)

A three-channel resonating-group calculation is performed to study the effects of channel coupling on the properties of the ^{3}H$+\alpha$ system. The channels included are ^{3}H$+\alpha$, n$+^6$Li, and n$+^6$Li* channels, with ^{6}Li and ^{6}Li* described by $(1s)^4(1p)^2$ harmonic-oscillator functions representing d$+\alpha$ cluster configurations with relative orbital angular momenta equal to 0 and 2, respectively. By comparing with the ^{3}H$+\alpha$ single-channel result, it is found that the three-channel calculation improves the $L=1$ ground state energy by 0.68 MeV and yields additional features such as cusps in the $L=0$ and 2 phase shifts and a dispersionlike resonance structure in the $L=1$ phase shift. In addition, it is noted that, in states with larger L values, the n$+^6$Li* aligned configurations make particularly important contributions. Characteristics of nucleon-exchange terms have also been briefly investigated; here one finds that, as far as the ^{3}H$+\alpha$ system is concerned, the important one-exchange and core-exchange contributions are only weakly affected by the presence of other channels.

[NUCLEAR REACTIONS ^{3}H(α,n)^{6}Li, ^{3}H(α,n)^{6}Li*. Effects of channel coupling. Resonating-group method with ^{3}H $+\alpha$, n $+$ ^{6}Li, and n $+$ ^{6}Li* channels.]

I. INTRODUCTION

The resonating-group method (RGM) was proposed by Wheeler[1] more than forty years ago. Since then, it has been extensively employed to study bound-state, scattering, and reaction problems especially in light systems.[2] Because of computational complexities associated with the necessity of taking into exact account the antisymmetrization of the wave function and the center-of-mass motion, it was generally thought that the domain of applicability of this method must be quite limited; indeed, it has been emphatically stated by some authors[3] about ten years ago that, from a practical standpoint, it can only be applied to very light systems with $A \leq 8$. As is now well known, this viewpoint turned out to be much too pessimistic. In the early and mid-seventies, several generator-coordinate methods began to be developed.[4] With these computational techniques, it was soon found that RGM calculations are feasible in even much heavier systems. In fact, a large number of such calculations now exist,[4] and much information has been obtained to advance our knowledge concerning the clustering properties of nuclei and the characteristics of internuclear interactions.

For detailed and systematic investigations, however, it is our opinion that, because of limitations imposed by present-day computational facilities, major efforts should still be concentrated on very light systems. Among these,

the seven-nucleon system is likely the most interesting one from the following viewpoints: (i) for the ^{3}H $+ \alpha$ configuration, core-exchange effects are very important because the interacting nuclei have a small nucleon-number difference,[5] and (ii) the interplay of different cluster structures, such as the ^{3}H $+ \alpha$, n $+$ ^{6}Li, and n $+$ ^{6}Li* structures, may be quite significant in this system. In addition, it is of course known that the ^{3}He(α,γ)^{7}Be reaction is relevant to the solar neutrino problem.[6,7] Quite clearly, a better understanding of the structure of the seven-nucleon system would lead to a more reliable estimate of the capture rate for this reaction.

In this investigation, we shall make a resonating-group study of the seven-nucleon system by taking ^{3}H $+ \alpha$, n $+$ ^{6}Li, and n $+$ ^{6}Li* channels into account, with ^{6}Li and ^{6}Li* being $T=0$ states described by $(1s)^4(1p)^2$ harmonic-oscillator shell-model functions representing d $+ \alpha$ cluster configurations with relative orbital angular momenta I equal to 0 and 2, respectively. For clarity in presentation, the discussion will be centered on the ^{3}H $+ \alpha$ channel; in other words, we shall be mainly concerned with the coupling or specific distortion effects of the n $+$ ^{6}Li and n $+$ ^{6}Li* channels on the bound-state and phase-shift properties of the ^{3}H $+ \alpha$ system.

Specific distortion effects on the bound and resonance states of the ^{3}H $+ \alpha$ system have previously been considered by other authors.[8,9] The results obtained showed

that, with such effects taken into account, there is a gain of about 0.7 MeV for the cluster separation energy in the ground state of the compound system. This is an interesting finding, since the corresponding gains in the $\alpha + \alpha$ and $d + \alpha$ systems are equal to about 0.3 and 1.7 MeV, respectively,[10,11] indicating that the importance of specific distortion effects can be correlated with the compressibilities of the clusters under consideration. In this calculation, we shall consider the effects of channel coupling not only on the bound and resonance states to verify the above-mentioned result, but also on the scattering phase shifts in order to obtain information concerning the reaction mechanism.

The present investigation of channel-coupling effects is undertaken also to supplement our recent three-cluster resonating-group study in which the influence of $d + \alpha$ surface clustering on the properties of the $n + {}^6\text{Li}$ system was examined.[12] It is our hope that with the knowledge learned from this and the previous investigation, we can gain a clear picture about the level structures and the reaction mechanism in the seven-nucleon system.

It should be mentioned that, as has been emphasized many times previously,[2] the Pauli principle has the effect of reducing greatly the differences between seemingly different cluster structures when the nucleons are close to one another. Thus, especially in the low-excitation region, it is a good approximation to omit other cluster configurations, such as $d + {}^5\text{He}$, $n + {}^6\text{Li}^*$ ($T = 1$), and so on.[13] We are confident that the present three-channel study is sufficiently extensive for our purpose.

In Sec. II we give a brief description of the resonating-group coupled-channel formulation. The results are discussed in Sec. III, where channel-coupling effects on the energies of the bound and resonance states, and on the characteristics of the scattering phase shifts in the ${}^3\text{H} + \alpha$ system will be considered. Finally, in Sec. IV, we summarize the findings of this investigation and make some concluding remarks.

II. FORMULATION

The formulation of a coupled-channel resonating-group calculation has already been described in Ref. 4; hence only a brief description will be given here. Because the nucleon-nucleon potential to be adopted is purely central, both the total orbital angular momentum L and the total spin angular momentum S are good quantum numbers. The value of S will be taken as $\frac{1}{2}$ since, as was mentioned in the Introduction, the emphasis of this investigation is to study the effects of channel coupling on the incident ${}^3\text{H} + \alpha$ channel.

Denoting the ${}^3\text{H} + \alpha$, $n + {}^6\text{Li}$, and $n + {}^6\text{Li}^*$ channels as channels 1, 2, and 3, respectively, we write the trial wave function in a particular L state with magnetic quantum number M as

$$\psi_L^M = \sum_i \psi_{iL}^M, \quad i = 1,2,3 \tag{1}$$

where

$$\psi_{1L}^M = \mathscr{A} \left\{ \phi_\alpha \phi_t \frac{1}{R_1} f_{1L}(R_1) Y_L^M(\hat{R}_1) \xi_S Z(\vec{R}_{\text{c.m.}}) \right\}, \tag{2}$$

$$\psi_{2L}^M = \mathscr{A} \left\{ \left[\phi_6(I=0) \frac{1}{R_2} f_{2l}^L(R_2) Y_l(\hat{R}_2) \right]_L^M \tilde{\xi}_S Z(\vec{R}_{\text{c.m.}}) \right\}, \tag{3}$$

$$\psi_{3L}^M = \sum_l \mathscr{A} \left\{ \left[\phi_6^*(I=2) \frac{1}{R_3} f_{3l}^L(R_3) Y_l(\hat{R}_3) \right]_L^M \right. $$
$$\left. \times \tilde{\xi}_S Z(\vec{R}_{\text{c.m.}}) \right\}, \tag{4}$$

with $\mathscr{A}$ being an antisymmetrization operator, ξ_S and $\tilde{\xi}_S$ being appropriate spin-isospin functions, $Z(\vec{R}_{\text{c.m.}})$ being any normalizable function describing the motion of the total c.m., and $\vec{R}_i$ ($i = 1,2,3$ with $\vec{R}_2 = \vec{R}_3$) representing the vector separation distance between the clusters. The relative orbital angular momentum l is coupled with the internal orbital angular momentum I to yield the desired value of L. As is evident, l is equal to L in the $n + {}^6\text{Li}$ channel (channel 2); however, in the $n + {}^6\text{Li}^*$ channel (channel 3), l will assume the value 2 for $L = 0$, 1 and 3 for $L = 1$, and $L - 2, L$, and $L + 2$ for $L \geq 2$.

The functions ϕ_α and ϕ_t describe the internal spatial structures of the α and ${}^3\text{H}$ clusters, respectively. They are chosen to have the lowest configurations in harmonic-oscillator wells. To simplify the calculation, we adopt a common value α of 0.44 fm^{-2} for their respective width parameters. This latter value is chosen such that the sum of the experimentally determined mean-square matter radii of the α particle and the triton is reproduced. The functions ϕ_6 and ϕ_6^* represent the spatial structures of ${}^6\text{Li}$ in its ground and excited states; as has already been mentioned, these will be taken as $(1s)^4(1p)^2$ harmonic-oscillator functions describing $d + \alpha$ cluster configurations with internal orbital angular momenta I equal to 0 and 2, respectively. Again, for the sake of reducing computational effort, we shall make the simplifying assumption of choosing the width parameter of the oscillator well to be the same as that for the α and ${}^3\text{H}$ clusters, namely, 0.44 fm^{-2}.

The linear variational amplitudes or relative-motion functions f_{1L}, f_{2L}^L, and f_{3l}^L are obtained by solving the projection equation

$$\langle \delta \psi_{iL}^M \mid H - E_T \mid \psi_L^M \rangle = 0, \tag{5}$$

where E_T is the total energy of the system and H is a Galilean-invariant Hamiltonian operator given by

$$H = \sum_{i=1}^7 T_i + \sum_{i<j=1}^7 V_{ij} - T_{\text{c.m.}}, \tag{6}$$

with V_{ij} being a nucleon-nucleon potential and $T_{\text{c.m.}}$ being the kinetic energy operator of the total center of mass. Following the procedure outlined in Ref. 4, one readily finds that these functions satisfy a set of coupled integro-differential equations. For example, in the $L = 3$ state, the

number of such equations in this set is five, involving the relative-motion functions f_{13}, f_{23}^3, f_{31}^3, f_{33}^3, and f_{35}^3. In each of these integro-differential equations, there appear, in addition to the direct potential, kernel terms which represent the nonlocal interaction and the coupling to other channels. The derivation of these kernel terms is quite complicated and a brief discussion of it, together with a description of a new calculational method for evaluating RGM matrix elements with Gaussian functions, is given in the Appendices.

The nucleon-nucleon potential employed in this investigation is purely central; it has the form[11]

$$V_{ij} = \left[V_R + \frac{1+P_{ij}^\sigma}{2} V_t + \frac{1-P_{ij}^\sigma}{2} V_s \right] \left[\frac{u}{2} + \frac{2-u}{2} P_{ij}^r \right] ,$$

(7)

where u is an exchange-mixture parameter, chosen in a way to be discussed below. The potentials V_R, V_t, and V_s are taken to have the following Gaussian forms:

$$V_R = V_{0R} \exp[-\kappa_R (\vec{r}_i - \vec{r}_j)^2] ,$$

$$V_t = - V_{0t} \exp[-\kappa_t (\vec{r}_i - \vec{r}_j)^2] ,$$

(8)

$$V_s = - V_{0s} \exp[-\kappa_s (\vec{r}_i - \vec{r}_j)^2] ,$$

with

$$V_{0R} = 200.0 \text{ MeV}, \quad \kappa_R = 1.487 \text{ fm}^{-2} ,$$

$$V_{0t} = 178.0 \text{ MeV}, \quad \kappa_t = 0.639 \text{ fm}^{-2} ,$$

(9)

$$V_{0s} = 91.85 \text{ MeV}, \quad \kappa_s = 0.465 \text{ fm}^{-2} .$$

This particular nucleon-nucleon potential is chosen because it yields a satisfactory description of not only the two-nucleon low-energy scattering data but also the essential properties of the deuteron, ^{3}H, and α particle.

As is noted from Eq. (7), we have further simplified the calculation by omitting the Coulomb interaction. This is a reasonable assumption to make, since our main objective is to study the influence of channel coupling on the properties of the ^{3}H + α system. It is certainly to be expected that the coupling of the channels should be affected more by the nuclear interaction than by Coulomb effects.

The coupled integro-differential equations are solved by a variational technique discussed by Kamimura.[14] From the resultant relative-motion functions, we extract the diagonal element $S_{L,L}^L$ and the off-diagonal element $S_{II,L}^L$ of the scattering matrix.[15] As is customary, the diagonal element will be parametrized as

$$S_{L,L}^L = \eta_{L,L}^L \exp(2i\delta_{L,L}^L) ,$$

(10)

in terms of the reflection coefficient $\eta_{L,L}^L$ and the phase shift $\delta_{L,L}^L$. For the coupling or off-diagonal element $S_{II,L}^L$, only the result for the transmission coefficient, defined as

$$\eta_{II,L}^L = | S_{II,L}^L | ,$$

(11)

will be needed in the following discussion.

III. RESULTS

A. Determination of the exchange-mixture parameter u

The exchange-mixture parameter u in the nucleon-nucleon potential is determined by using experimental data on the ^{3}H + α cluster separation energies in the $\frac{3}{2}^-$ ground and the $\frac{1}{2}^-$ first excited states.[16] By averaging these energies according to $\langle \vec{L} \cdot \vec{S} \rangle$ weighting and by further adding a Coulomb energy of 0.86 MeV estimated by utilizing experimental results on the ground-state energies of ^{7}Li and ^{7}Be, it is found that, in a calculation where Coulomb and spin-orbit effects are not included, the ^{3}H + α relative energy in the lowest $L = 1$ state should be equal to -3.17 MeV. To obtain this latter value with our present three-channel formulation, we find that the value of u is 0.985.

With this value of u, we calculate the threshold energies of the n + ^{6}Li and n + ^{6}Li* channels. The results are shown in Fig. 1, where it is seen that the calculated values are larger than the experimental values by about 2 MeV.

B. Effects of channel-coupling on bound and resonance states

Channel-coupling effects on the $L = 1$ bound state and $L = 3$ resonance state are shown in Fig. 1, where the columns labelled by SC (single channel), CC (coupled channel), and Full represent, respectively, results obtained with the ^{3}H + α channel alone, with the ^{3}H + α plus n + ^{6}Li channels, and with all three channels included. As is well known, these particular states can be reasonably well described by a single t + α cluster configuration[2]; even so, however, we note that there is a substantial improvement when the n + ^{6}Li and n + ^{6}Li* channels are taken into consideration. For the $L = 1$ ground state, the energy is mainly improved by the inclusion of the n + ^{6}Li channel; further addition of the n + ^{6}Li* channel seems to
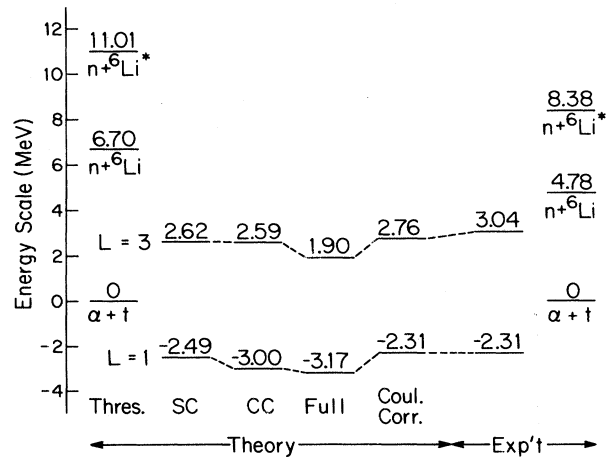

FIG. 1. Comparison of $L = 1$ ground-state energies and $L = 3$ resonance-state energies obtained with the single-channel (SC), coupled-channel (CC), and full (Full) calculations. Calculated and experimental threshold energies for the various channels are also shown.

have much less influence. The opposite turns out to be the case for the $L=3$ resonance state. Here the calculation shows that there is only a minor difference between the SC and CC results and the improvement in the $L=3$ resonance energy comes almost entirely as a consequence of the presence of the n + ^{6}Li* channel.

The above observation concerning the roles of the n + ^{6}Li and n + ^{6}Li* channels in the $L=1$ and 3 states can be easily understood. In the $L=1$ state, the relative orbital angular momentum l has the same value equal to 1 in both channels. On the other hand, in the $L=3$ state, l is equal to 3 in the n + ^{6}Li channel, but may have a smaller value equal to 1 in the n + ^{6}Li* channel (i.e., the aligned configuration). This means that the neutron can come closer to ^{6}Li* than to ^{6}Li; consequently, when the value of L is large, one expects the n + ^{6}Li* channel to have a larger influence.

The energy values obtained with the SC and the full calculations differ by 0.68 and 0.72 MeV in the $L=1$ and 3 states, respectively. The fact that the improvement in the $L=3$ state is even larger than that in the $L=1$ state has also been found by Mihailović and Poljšak[9] in their cluster-model study of ^{7}Li. If one now makes a further Coulomb-energy correction of 0.86 MeV, then the calculated $L=3$ resonance occurs at 2.76 MeV which agrees rather well with the value of 3.04 MeV determined from experimental data by $\langle \vec{L} \cdot \vec{S} \rangle$ weighting.

It is interesting to compare the results obtained here with those obtained by other authors. In the cluster-model study of Beck et al.,[9] the cluster configurations included are the two-cluster configuration ^{3}H + α, and the three-cluster configurations n + α + d($T=0$) and n + α +d($T=1$) with the d + α relative orbital angular momentum chosen to be equal to 0. The result showed that, for the $L=1$ ground state, the energy obtained with the full calculation is 0.66 MeV better than that obtained with a single-channel ^{3}H + α calculation. In the investigation carried out by Kanada et al.,[8] specific distortion effects in the ^{3}H + α system are taken into consideration by the introduction of an ^{3}H* + α channel. This resulted in an improvement of 0.76 MeV for the ground-state energy. The important point to note is that, in these three calculations where apparently different cluster structures are considered together with the ^{3}H + α configuration, the energy gain in the $L=1$ ground state is approximately the same and equal to about 0.7 MeV.[17] At first, this may seem to be a surprising finding, but is actually rather to be expected. It is merely a demonstration of the fact that the procedure of antisymmetrization has the effect of reducing, to a large extent, the differences between apparently different nonorthogonal cluster functions.

For the $L=3$ resonance state, the situation is somewhat different. Our present investigation shows that the introduction of channel coupling improves the energy by 0.72 MeV, which is significantly larger than the improvement of 0.33 MeV obtained by Kanada et al.[8] This indicates that, in a state where L is large, a better description can be obtained by adding into the formulation n + ^{6}Li and n + ^{6}Li* configurations rather than the ^{3}H* + α configuration. Evidently, the reason must be that the important n + ^{6}Li* aligned configuration cannot be properly taken

into account in a calculation involving only ^{3}H + α and ^{3}H* + α channels.

C. Effects of channel-coupling on S-matrix elements

The results for the phase shift $\delta_{L,L}^L$, the reflection coefficient $\eta_{L,L}^L$, and the transmission coefficient $\eta_{II,L}^L$ in states with $L=0$–7 are shown in Figs. 2–8 as a function of E, the relative energy of the ^{3}H and α clusters in the c.m. system. For the phase shift, we show the values obtained in the single-channel case (SC, dashed curves), the coupled-channel case (CC, solid circles), and the full calculation (Full, solid curves), while for the reflection and transmission coefficients, only the values obtained in the full calculation are plotted. Also, for clarity in presentation, we shall not show the transmission coefficient for transition into any weakly coupled (II) state where its value is smaller than 0.1 in the entire range of relative energy considered (i.e., 0–35 MeV).

The salient features in each of these L states are as follows.

(i) $L=0$ state (Fig. 2). The most notable feature is that the phase-shift curve has a cusp at the n + ^{6}Li threshold. This is an expected phenomenon,[18] and arises from the fact that the ^{3}H + α configuration is coupled rather strongly to a neutron channel with $l=0$.[19] At present, there is some experimental evidence for this behavior. Empirical ^{3}H + α phase-shift values in the $L=0$ state (see Fig. 3 of Ref. 8) do seem to deviate from a monotonically decreasing trend at the n + ^{6}Li threshold of 4.78 MeV. It would indeed be interesting to reanalyze the experimental data by specifically keeping the presence of an $L=0$ phase-shift cusp in mind. Such a precautionary measure may very well lead to a more successful phase-shift analysis of the measured results.

The calculation of Kanada et al. suffers from the fact that specific distortion effects are taken into account by the introduction of a fictitious ^{3}H* + α cluster configuration. This latter configuration consists of charged clusters and has a high energy threshold of 18.42 MeV. As a result, no phase-shift cusp appears in their investigation which covers an energy range up to about 15 MeV and the influence of specific distortion was found to be quite minor in the $L=0$ state. Thus, even though their calculation is technically more convenient and the result obtained for the $L=1$ ground state is quite satisfactory, our opinion is that a better way to study specific distortion effects in all L states is by introducing realistic cluster configurations according to energetical considerations.

From Fig. 2, one readily sees that, especially at lower energies, the ^{3}H + α channel is coupled more strongly to the n + ^{6}Li channel than to the n + ^{6}Li* channel. Evidently, this is related to the fact that the relative orbital angular momentum l is equal to 0 in the n + ^{6}Li case but equal to 2 in the n + ^{6}Li* case; hence the coupling between the ^{3}H + α and the n + ^{6}Li* channels is reduced because of centrifugal-barrier effects.

(ii) $L=1$ state (Fig. 3). With the full three-channel calculation, the result shows that there appears at about 0.6 MeV above the n + ^{6}Li* threshold an $L=1$ resonance level which does not show up in a SC calculation. From the dispersionlike behavior of the phase shift, one can con-
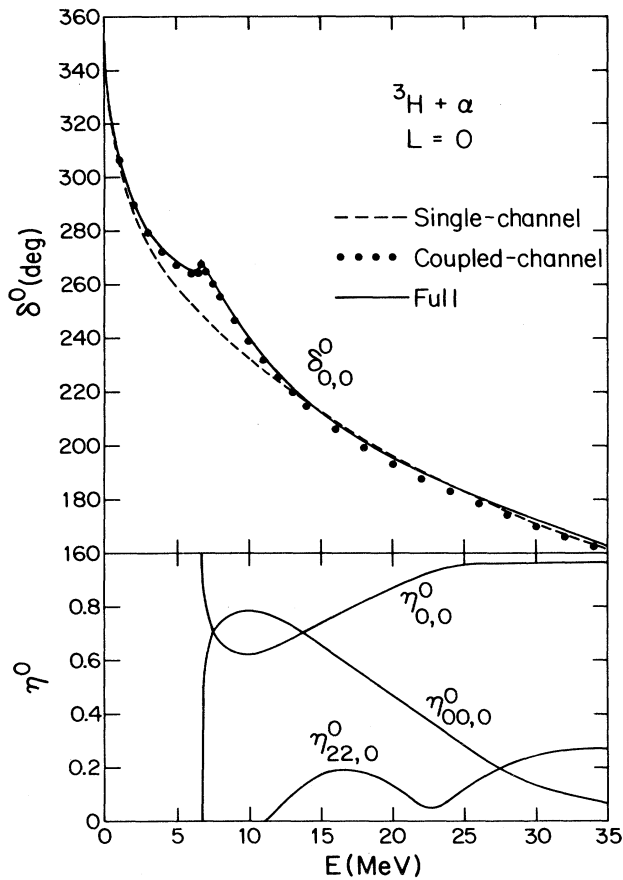
FIG. 2. Calculated phase shifts, reflection coefficient, and transmission coefficients for $L = 0$ in the ^{3}H$+\alpha$ channel. The dashed curve, solid circles, and solid curve represent results obtained with the SC, CC, and full calculations, respectively.
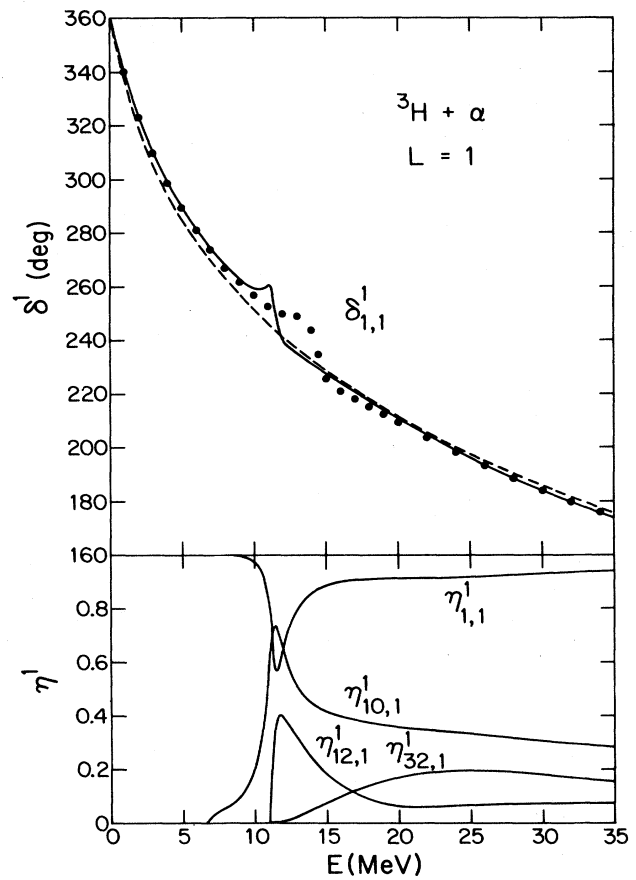
FIG. 3. Same as Fig. 2, except that $L = 1$.

clude[2] that the partial width for the decay into the ^{3}H $+ \alpha$ channel is much smaller than the total width of this level. In fact, by studying the energy-dependent behavior of the S-matrix elements, it can be easily determined that at this resonance the nucleus ^{7}Li has mainly a n $+$ ^{6}Li* cluster configuration with $l = 1$.

Although there is little doubt that such a resonance level exists, one should be careful about the quantitative aspects of the result. In our calculation, the nucleus ^{6}Li* is described by a simple $(1s)^4(1p)^2$ configuration which does not allow for a sufficient degree of d $+ \alpha$ clustering. As has been found in a recent single-channel study of the n $+$ ^{6}Li system,[12] an adequate allowance for such clustering can increase the $l = 1$ resonance energy by about 2.5 MeV. Thus it is reasonable to expect that this level may actually possess an excitation energy of around 12 MeV. Experimentally,[16] only scant information concerning the level structure of ^{7}Li is known in the excitation-energy region beyond 11 MeV and, hence no identification with experiment can be made for this level at the present moment.

(iii) $L = 2$ state (Fig. 4). From Fig. 4 one notes that, in the $L = 2$ state, both the n $+$ ^{6}Li and the n $+$ ^{6}Li* channels contribute in modifying the phase-shift result of the

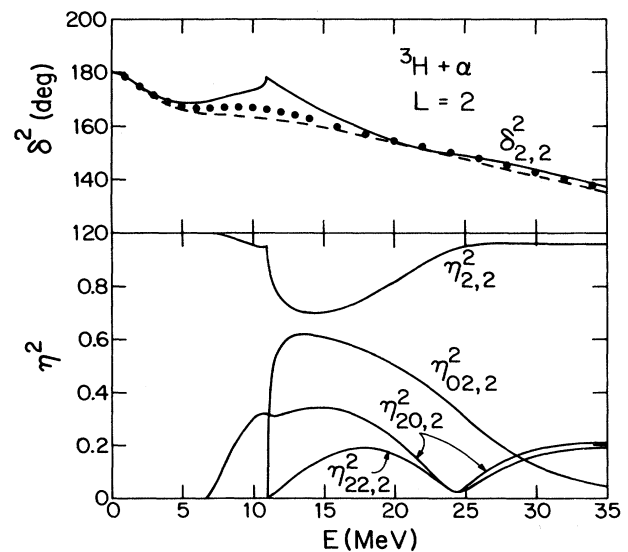
FIG. 4. Same as Fig. 2, except that $L = 2$.

SC calculation. With the n + ^{6}Li channel taken into consideration, it is seen that the very broad $L = 2$ state at about 10 MeV, discussed previously in a SC ^{3}H + α study,[20] becomes somewhat more evident.

As expected, there appears a prominent cusp in the $L = 2$ phase-shift curve, due to the coupling of the ^{3}H + α channel with the n + ^{6}Li* channel in the $l = 0$ state. At present, we can find no definitive evidence for the existence of this cusp, because the existing $L = 2$ empirical phase-shift values are not refined enough to serve this purpose.

(iv) $L = 3$ state (Fig. 5). In the low-energy region around the sharp $L = 3$ resonance, it is noted that the ^{3}H + α phase shift is mainly affected by the coupling to the n + ^{6}Li* aligned configuration. The presence of the n + ^{6}Li cluster configuration in the calculation seems to have little significance.

At higher energies above 12 MeV, the situation is somewhat changed. Here one finds that the n + ^{6}Li channel does seem to have some influence. In addition, it is seen from Fig. 5 that, of all the transmission coefficients, $\eta^3_{30,3}$ has the largest value, and for the n + ^{6}Li* channel the coupling of the ^{3}H + α channel to the $l = 3$ configuration is even stronger than that to the $l = 1$ aligned configuration. To understand these findings, one needs only to note that, in the Pauli-favored $l = 3$ state, a SC n + ^{6}Li calculation yields a broad resonance behavior in the energy region around 15 MeV above the n + ^{6}Li threshold.[12] The presence of such resonance structures in the n + ^{6}Li and
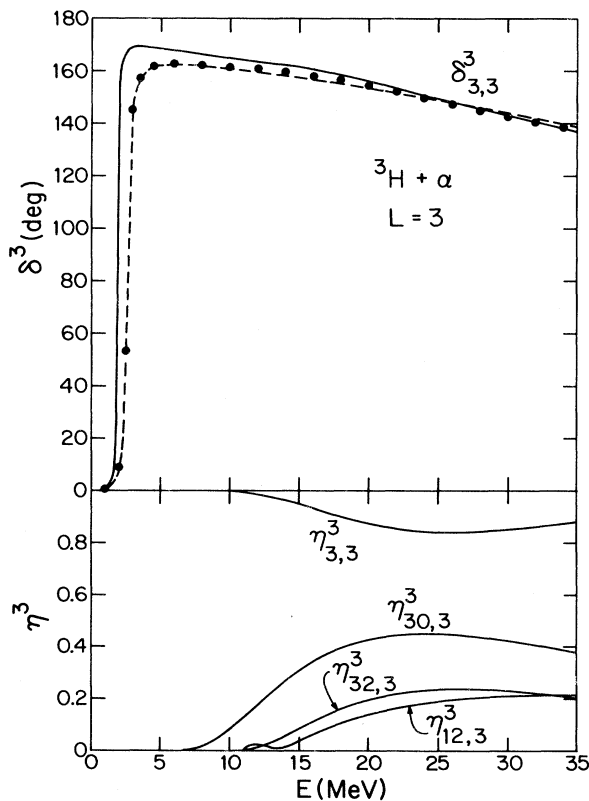

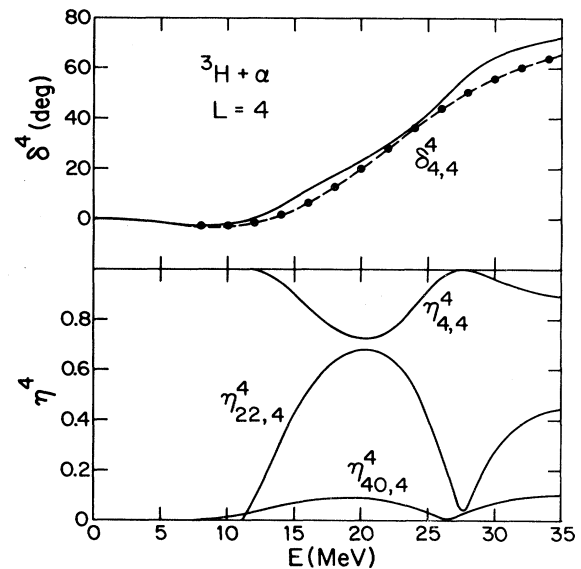FIG. 6. Same as Fig. 2, except that $L = 4$.

n + ^{6}Li* channels is responsible for the features of channel coupling mentioned above.

(v) $L = 4$ and 5 states (Figs. 6 and 7). In these orbital angular momentum states, the phase-shift and transmission-coefficient results show that the ^{3}H + α channel couples rather strongly to the aligned configurations (i.e., $l = L - 2$) of the n + ^{6}Li* channel, but very weakly to the n + ^{6}Li channel. This is quite definitely a consequence of the different centrifugal barriers in these respective configurations.

As is seen from Figs. 6 and 7, the effect of channel coupling on the ^{3}H + α phase shifts is fairly substantial in the energy region considered here. This is related to the fact that, at energies around 22 MeV, there exist broad $L = 4$ and 5 resonance levels which have predominantly a
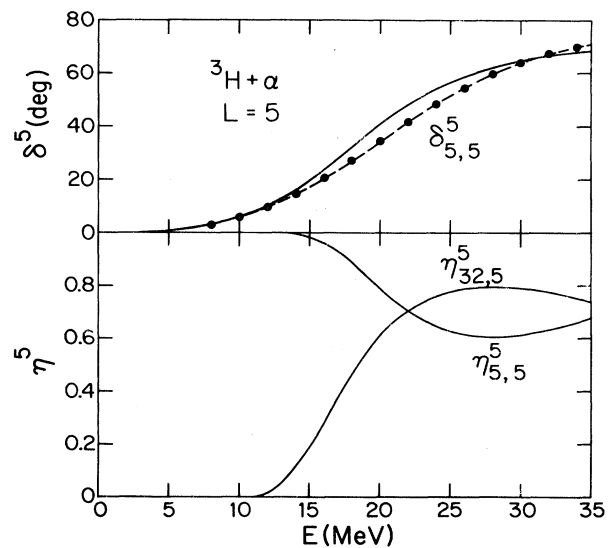

FIG. 5. Same as Fig. 2, except that $L = 3$.

FIG. 7. Same as Fig. 2, except that $L = 5$.

^{3}H + α cluster structure.[20] In the $L = 4$ state, one further notes that there appears a wavy behavior in the phase-shift curve obtained from the full calculation. This can be understood as resulting from the presence of a broad $l = 2$ resonance with a n + ^{6}Li* cluster configuration.

At energies higher than 35 MeV, the channel-coupling effect becomes progressively weaker. In the $L = 4$ state, for example, the phase shifts obtained at 50 MeV with the SC and the full calculations are equal to 73.6° and 74.6°, respectively, a difference of only 1°.

(vi) $L = 6$ and 7 states (Fig. 8). For completeness, we show in Fig. 8 the $L = 6$ and 7 results obtained with the full calculation. Because of high centrifugal barriers, the coupling between the channels is weak and the aligned configurations of the n + ^{6}Li* channel yield again the most significant contributions.

(vii) Summary. The purpose of this investigation is to examine, in the incident ^{3}H + α channel, the effects arising from the coupling with the n + ^{6}Li and n + ^{6}Li* channels. In spite of the fact that both the ^{3}H and the α clusters have comparatively low compressibilities, the result shows that channel-coupling effects are important and should be properly taken into consideration. With the full three-channel calculation, we find that there appear interesting cusp behavior, additional resonances, and a substantial modification of the phase-shift and binding-energy values.

Both n + ^{6}Li and n + ^{6}Li* channels are found to make important contributions. At higher L values, it is shown that the aligned configurations of the n + ^{6}Li* channel are particularly important. This indicates that, in any future investigation where one wishes to improve the single-channel results by introducing additional $A + B$ cluster configurations, it is important that all states of A or B arising from the same intrinsic structure must be included in the calculation.

The importance of the n + ^{6}Li* channel is further demonstrated in Fig. 9 where we plot the calculated cross sections σ_R and σ_R^* for the ^{4}He(^{3}H,n)^{6}Li and ^{4}He(^{3}H,n)^{6}Li* reactions, respectively. Here one sees that
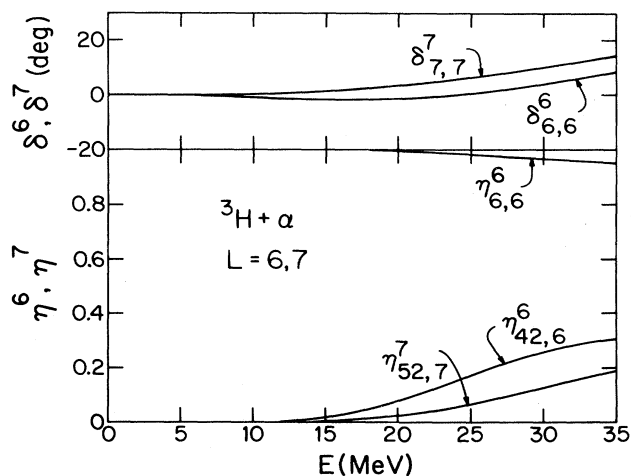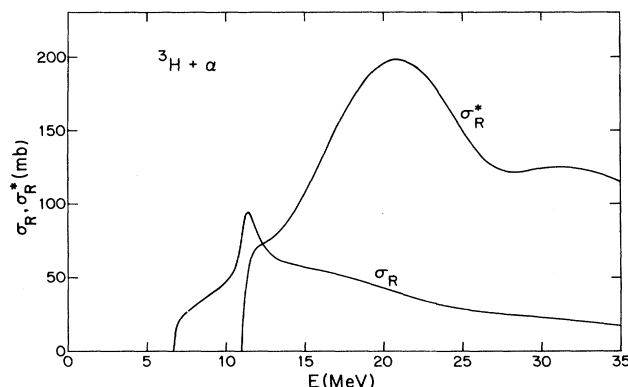
FIG. 9. Calculated cross sections σ_R and σ_R^* for the ^{4}He(^{3}H,n)^{6}Li and ^{4}He(^{3}H,n)^{6}Li* reactions, respectively.

σ_R^* is generally much larger than σ_R. For instance, at 15.95 MeV, the ratio σ_R^*/σ_R is equal to 2.33, which is in good agreement with the measured value[13] for the ^{4}He(^{3}He,p) reactions leading to the ground and first excited states of ^{6}Li.

D. Effects of channel-coupling on exchange contributions

Antisymmetrization effects have been extensively studied by investigating the general characteristics of the exchange-kernel function which appears in a SC resonating-group formulation.[5] The main findings were (i) the one-exchange terms are generally important in all nuclear systems and over a wide energy range, and (ii) the core-exchange terms make important contributions when the nucleon-number difference of the interacting nuclei is small. A number of SC resonating-group studies in specific systems have subsequently been performed to quantitatively examine the contributions from various nucleon-exchange terms,[21] and the results obtained have fully supported these general findings.

In the ^{3}H + α case, the nucleon-number difference is small and, hence core-exchange effects are very significant, as has been verified in SC resonating-group studies of this system.[20] These exchange effects clearly manifest themselves through a zigzag pattern in the phase-shift result as a function of L,[20,22] and through a characteristic rapid rise of the differential cross section in the backward angular region at a relatively high energy. From a macroscopic viewpoint, the main consequence of such effects is that, in constructing an effective local internuclear potential, one must take care by including at least the freedom of having an odd-even l-dependent or parity-dependent component. In this investigation, our purpose is to determine whether the presence of channel coupling can significantly modify the extent of the nucleon-exchange contributions. To achieve this purpose, we shall compare the results obtained with the SC and full calculations.

In Fig. 10, we show such a comparison for the phase shifts $\delta_{L,L}^L$ (abbreviated as δ_L) calculated at 35 MeV. Here the crosses and open circles represent results obtained with the SC and full calculations, respectively. As is seen, the difference is rather small; in comparing with the SC re-
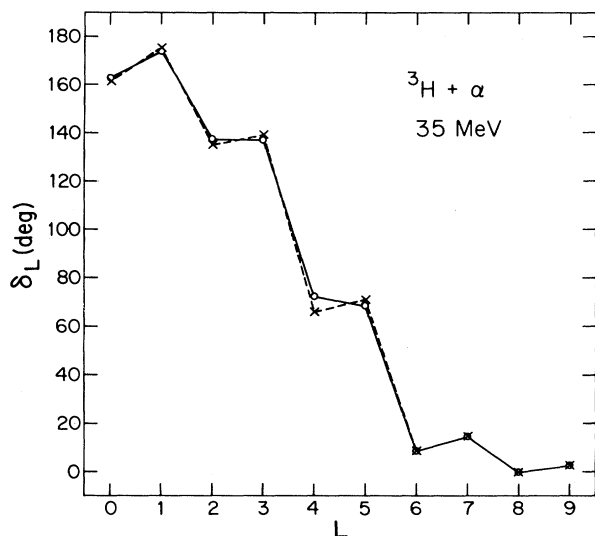

FIG. 8. Same as Fig. 2, except that $L = 6$ and 7.

FIG. 10. Comparison of the ^{3}H $+ \alpha$ phase shifts at 35 MeV, obtained with the SC (crosses) and full (open circles) calculations.

sult, the full calculation yields slightly larger phase shifts in even-L states and slightly smaller phase shifts in odd-L states. This indicates that, for the ^{3}H $+ \alpha$ system, the coupling to the n $+$ ^{6}Li and n $+$ ^{6}Li* channels reduces slightly the core-exchange contributions but has almost no effect on the one-exchange contributions.

More detailed information is contained in the Argand plot of the 35-MeV S-matrix element $S_{L,L}^L$ (abbreviated as S_L) shown in Fig. 11, where the symbols have the same meaning as explained in the preceding paragraph. In such a plot, the odd-even effect shows up through a bunching of the odd-l and even-l points. By examining this figure, one can clearly see that this effect is still very strong in the full calculation.
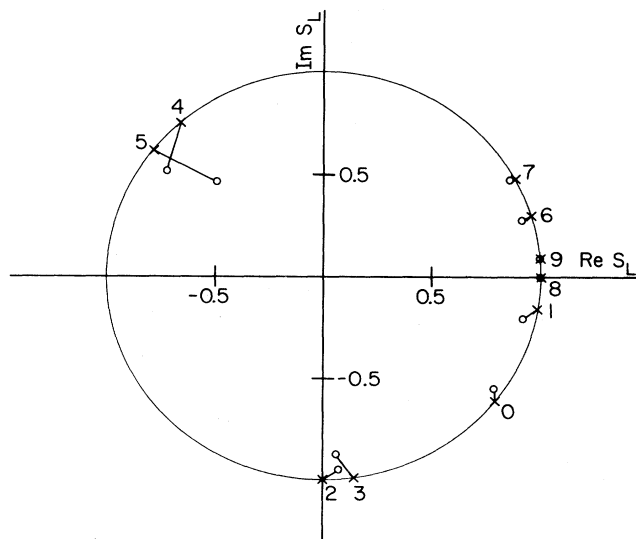

FIG. 11. Argand plots of the 35-MeV S-matrix element S_L, obtained with the SC (crosses) and full (open circles) calculations.
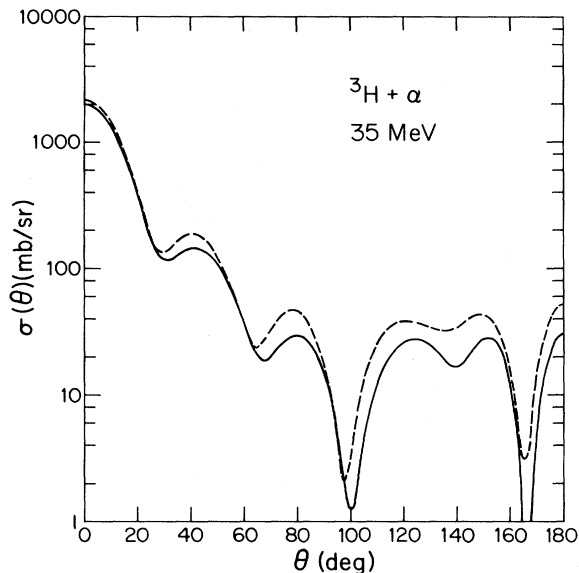

FIG. 12. Comparison of ^{3}H$+\alpha$ differential cross sections at 35 MeV, obtained with the SC (dashed curve) and full (solid curve) calculations.

To complete the discussion, we show in Fig. 12 a comparison between the differential cross sections at 35 MeV obtained with the SC (dashed curve) and full (solid curve) calculations. Here one sees that, because of reaction effects, the solid curve lies generally below the dashed curve, which is an expected finding. However, it is also noted that the feature of cross-section rise in the backward angular region is equally prominent in both calculations, indicating again that core-exchange effects in the ^{3}H $+ \alpha$ system are not greatly influenced by the coupling to other channels.

IV. CONCLUSIONS

In this investigation, a three-channel resonating-group calculation, consisting of ^{3}H $+ \alpha$, n $+$ ^{6}Li, and n $+$ ^{6}Li* cluster configurations, has been performed. The main purpose is to study the effect of channel coupling on the properties of the energetically most-favored ^{3}H $+ \alpha$ configuration. To achieve this purpose, we have carried out a systematic examination by completing not only the full calculation involving all three channels, but also a single-channel calculation with the ^{3}H $+ \alpha$ channel alone and a coupled-channel calculation consisting of ^{3}H $+ \alpha$ and n $+$ ^{6}Li channels.

In comparing with the single-channel result, the full three-channel calculation lowers both the $L = 1$ ground-state energy and the $L = 3$ resonance state energy by about 0.7 MeV. The ground-state energy is improved mainly by the inclusion of the n $+$ ^{6}Li channel, with the addition of the n $+$ ^{6}Li* channel yielding a smaller gain. On the other hand, for the $L = 3$ resonance state, the opposite turns out to be true.

Both the n + ^{6}Li and n + ^{6}Li* channels are significant in modifying the ^{3}H + α single-channel scattering result. With the full calculation, we find such new features as cusps in the $L = 0$ and 2 phase shifts and dispersionlike resonance behavior in the $L = 1$ phase shift. In addition, it is noted that, in states with larger L values, the n + ^{6}Li* aligned configurations make particularly important contributions.

Characteristics of nucleon-exchange terms have also been briefly investigated. Here one finds that, as far as the ^{3}H + α system is concerned, the important one-exchange and core-exchange contributions are both only weakly affected by the inclusion of other channels. This is a very significant finding, since it indicates that the general conclusions[5,21] about exchange effects, reached previously by examining the properties of the kernel function in a single-channel resonating-group formulation, are valid and can be used to predict the importance of exchange contributions in complicated systems.

At this moment, we wish to make some comments about the types of cluster configurations which should be included in a multichannel resonating-group study. Although the Pauli principle has the effect of reducing the differences between apparently different many-nucleon configurations, it would still be important to have some guide as to the most appropriate choice in an approximate calculation. From a practical viewpoint, this will certainly be useful, since it is well known that multichannel resonating-group calculations are complicated to formulate and, hence the number of cluster configurations should be chosen as small as possible in order to make the investigation computationally feasible. Based on the knowledge gained in present and previous[8,9] calculations in the seven-nucleon system, it seems to us that the selection criteria should be as follows: (i) cluster configurations should be chosen according to energetical considerations, and (ii) all states of the constituent clusters with the same intrinsic structure should be taken into account. In the calculation of Kanada et al.,[8] the cluster configurations adopted are the ^{3}H + α and ^{3}H* + α configurations and the above criteria are not met; hence although their results for the ground-state energy and for the phase shifts in the low-energy region are quite reasonable, certain defects do show up, as has been pointed out in the preceding section.

In conclusion, we have learned from this investigation the essential features of channel coupling. As our future project, we plan to carry out the difficult task of extending our present calculation to include target-clustering, Coulomb, and absorption effects, with the hope of eventually explaining the main features of all the low- and medium-energy experimental data which exist in the seven-nucleon system.

APPENDIX A: COUPLING KERNELS IN GENERATOR COORDINATE SPACE

In this Appendix, we show the expressions of the kernel functions derived with the generator-coordinate method (i.e., GCM kernels). Both the kernels for the n + ^{6}Li system[23] and the coupling terms between the ^{3}H + α and n + ^{6}Li channels will be given. For the derivation of these kernels, the internal wave function of ^{6}Li is assumed to be a simple shell-model wave function with SU_4 label (20) and a common harmonic oscillator width parameter α is used for all the constituent clusters.

For our purpose, we introduce an ^{6}Li, SU_3 coherent state by the expression[24]

$$\phi_{(20)}^{\hat{\omega}}(^6\text{Li}) \equiv \mathscr{R}(\hat{\omega})\phi_{(20)H}(^6\text{Li})$$

$$= \sum_{IM} A_{2I} \left[\frac{4\pi}{2I+1} \right]^{1/2} Y_{IM}^*(\hat{\omega})\phi_{(20)IM}(^6\text{Li}) ,$$

$$\text{(A1)}$$

where $\phi_{(20)H}(^6\text{Li})$ is the highest weight state defined by the internal wave function of the $(1s)^4(1p_z)^2$ configuration,[25] $\mathscr{R}(\hat{\omega})$ is a rotational operator with Euler angles specified by a unit vector $\hat{\omega}$, and

$$A_{NI} = (-1)^{(N-I)/2} \left[\frac{N!(2I+1)}{(N-I)!!(N+I+1)!!} \right]^{1/2} . \quad \text{(A2)}$$

Also, we define a localized Gaussian function

$$A_\gamma(\vec{r},\vec{z}) = \left[\frac{2\gamma}{\pi} \right]^{3/4} \exp[-\gamma(\vec{r} - \vec{z}/\sqrt{\gamma})^2 + \vec{z}^2/2] , \quad \text{(A3)}$$

which is a coherent state of harmonic-oscillator wave functions if we take $\vec{z}$ to be a complex variable. In the following, we further denote by $\mathcal{X}(n)$ the spin-isospin function of the incident neutron and use a factor $e(S)$, with $e(\frac{1}{2}) = -\frac{1}{2}$ and $e(\frac{3}{2}) = 1$, to represent the effect of spin-isospin coupling in each spin angular momentum state S [see the expressions of n + ^{6}Li(20) kernels given below].

Generating functions for Eqs. (2)—(4) are defined by[26]

$$\Phi^{\vec{z}}(^3\text{H}+\alpha) = \mathscr{A}'_{^3\text{H}+\alpha}[A_{\gamma'}(\vec{R}_1,\vec{z})\phi(^3\text{H})\phi(\alpha)] ,$$

$$\Phi^{\vec{z},\hat{\omega}}(\text{n}+^6\text{Li}) = \mathscr{A}'_{\text{n}+^6\text{Li}}[A_\gamma(\vec{R}_2,\vec{z})\phi_{(20)}^{\hat{\omega}}(^6\text{Li})\mathcal{X}(\text{n})] ,$$

$$\text{(A4)}$$

where $\gamma' = 6\alpha/7$ and $\gamma = 3\alpha/7$ are harmonic-oscillator constants for the relative motions in the ^{3}H + α and n + ^{6}Li channels, respectively, and $\mathscr{A}'_{^3\text{H}+\alpha}$ and $\mathscr{A}'_{\text{n}+^6\text{Li}}$ are normalized antisymmetrization operators. The nucleon-nucleon potential used to derive the kernel expressions is assumed to have the form

$$V(r) = V_0 \exp(-\kappa r^2)(W + BP_\sigma - HP_\tau - MP_\sigma P_\tau) . \qquad \text{(A5)}$$

In addition, the following constants are defined:

$$\tilde{V}_0 = V_0[\alpha/(\alpha + 2\kappa)]^{3/2}, \quad \eta = \kappa/(\alpha + 2\kappa) ,$$

$$\tilde{\kappa} = 7\eta/6, \quad \tilde{\kappa}' = 7\eta/12 , \qquad \text{(A6)}$$

$$X_d = 8W + 4B - 4H - 2M, \quad X_e = 8M + 4H - 4B - 2W ,$$

$$F_1 = W + B + H + M ,$$

and

$$F_4 = \begin{cases} 2W - B - H + M/2 \\ 2W + 2B - H - M , \end{cases}$$

$$F_5 = \begin{cases} W/2 - B - H + 2M \\ -W - B + 2H + 2M , \end{cases} \qquad \text{(A7)}$$

for

$$S = \begin{cases} \frac{1}{2} \\ \frac{3}{2} . \end{cases}$$

1. $n + {}^6\text{Li}(20)$ kernels

The normalization kernel is

$$\langle \Phi^{\vec{z}',\hat{\omega}'}(n + {}^6\text{Li}) \mid \Phi^{\vec{z},\hat{\omega}}(n + {}^6\text{Li}) \rangle = \exp(\vec{z}'^* \cdot \vec{z})(\hat{\omega}' \cdot \hat{\omega})^2 - \exp(-\vec{z}'^* \cdot \vec{z}/6) \times [(\hat{\omega}' \cdot \hat{\omega})^2 + \tfrac{7}{6} e(S)(\hat{\omega}' \cdot \hat{\omega})(\vec{z}'^* \cdot \hat{\omega})(\vec{z} \cdot \hat{\omega}')] .$$

The kinetic energy kernel is

$$\langle \Phi^{\vec{z}',\hat{\omega}'}(n + {}^6\text{Li}) \mid \sum_{i=1}^{7} T_i - T_{\text{c.m.}} \mid \Phi^{\vec{z},\hat{\omega}}(n + {}^6\text{Li}) \rangle$$

$$= E_u [\exp(\vec{z}'^* \cdot \vec{z})(\hat{\omega}' \cdot \hat{\omega})^2 \{ \tfrac{22}{3} - \tfrac{1}{3}(\vec{z}'^* - \vec{z})^2 \}$$

$$- \exp(-\vec{z}'^* \cdot \vec{z}/6) \{ (\hat{\omega}' \cdot \hat{\omega})^2 [\tfrac{22}{3} - \tfrac{1}{3}((\vec{z}'^*)^2 + \vec{z}^2) - \tfrac{1}{9} \vec{z}'^* \cdot \vec{z}]$$

$$+ \tfrac{7}{6} e(S)(\hat{\omega}' \cdot \hat{\omega})(\vec{z}'^* \cdot \hat{\omega})(\vec{z} \cdot \hat{\omega}')[8 - \tfrac{1}{3}((\vec{z}'^*)^2 + \vec{z}^2) - \tfrac{1}{9} \vec{z}'^* \cdot \vec{z}] \}] ,$$

where $E_u = 3\hbar^2 \alpha/(4M_n)$ with M_n being the nucleon mass.

The interaction kernel is

$$\langle \Phi^{\vec{z}',\hat{\omega}'}(n + {}^6\text{Li}) \mid \sum_{i<j}^{7} V_{ij} \mid \Phi^{\vec{z},\hat{\omega}}(n + {}^6\text{Li}) \rangle = \tilde{V}_0 \{ \exp(\vec{z}'^* \cdot \vec{z})[G^{(\text{in})} + G^{(d)}] - \exp(-\vec{z}'^* \cdot \vec{z}/6) \times [G_1^{(e)} + e(S)G_2^{(e)}] \} ,$$

where

$$G^{(\text{in})} = (\hat{\omega}' \cdot \hat{\omega})^2 [(2 - \eta)X_d + (1 + \eta)X_e + (1 - 2\eta + 2\eta^2)F_1] + \eta^2 F_1 ,$$

$$G^{(d)} = \exp\{ -\tilde{\kappa}(\vec{z}'^* + \vec{z})^2/2 \} [\tfrac{1}{2}(\hat{\omega}' \cdot \hat{\omega})^2 X_d + F_4 \{ (1 - \eta)(\hat{\omega}' \cdot \hat{\omega})^2 + \tfrac{7}{6}\eta^2(\hat{\omega}' \cdot \hat{\omega})[(\vec{z}'^* \cdot \hat{\omega}')(\vec{z} \cdot \hat{\omega}) + (\vec{z}'^* \cdot \hat{\omega})(\vec{z} \cdot \hat{\omega}')$$

$$+ (\vec{z}'^* \cdot \hat{\omega}')(\vec{z}'^* \cdot \hat{\omega}) + (\vec{z} \cdot \hat{\omega}')(\vec{z} \cdot \hat{\omega})] \}] ,$$

$$G_1^{(e)} = (\hat{\omega}' \cdot \hat{\omega})^2 \{ (\tfrac{3}{2} - \eta)X_d + (\tfrac{1}{2} + \eta)X_e + (1 - 2\eta + 2\eta^2)F_1 - (1 - \eta)F_4 - \eta F_5 \}$$

$$+ \eta^2 F_1 + [\exp(-\tilde{\kappa}(\vec{z}'^*)^2/2) + \exp(-\tilde{\kappa}\vec{z}^2/2)](\hat{\omega}' \cdot \hat{\omega})^2 [\tfrac{1}{2}(X_d + X_e) + (1 - \eta)F_4 + \eta F_5]$$

$$+ [\exp(-\tilde{\kappa}(\vec{z}'^*)^2/2)(\vec{z}'^* \cdot \hat{\omega}')(\vec{z}'^* \cdot \hat{\omega}) + \exp(-\tilde{\kappa}\vec{z}^2/2)(\vec{z} \cdot \hat{\omega}')(\vec{z} \cdot \hat{\omega})](\hat{\omega}' \cdot \hat{\omega})\tfrac{7}{6}\eta[\eta F_4 + (1 - \eta)F_5]$$

$$- \exp\{ -\tilde{\kappa}(\vec{z}'^* - \vec{z})^2/2 \}(\hat{\omega}' \cdot \hat{\omega}) \{ (\hat{\omega}' \cdot \hat{\omega})(\tfrac{1}{2}X_e + \eta F_5) + \tfrac{7}{6}F_5[(\eta \vec{z}'^* + (1 - \eta)\vec{z}) \cdot \hat{\omega}'][((1 - \eta)\vec{z}'^* + \eta \vec{z}) \cdot \hat{\omega}] \} ,$$

$$G_2^{(e)} = \tfrac{7}{6}(\hat{\omega}' \cdot \hat{\omega})(\vec{z}'^* \cdot \hat{\omega})(\vec{z} \cdot \hat{\omega}') \{ [\tfrac{1}{2}(3 - \eta)X_d + (1 + \tfrac{1}{2}\eta)X_e] + [\exp(-\tilde{\kappa}(\vec{z}'^*)^2/2) + \exp(-\tilde{\kappa}\vec{z}^2/2)]$$

$$\times [\tfrac{1}{2}((1 - \eta)X_d + \eta X_e) + (1 - 2\eta + 2\eta^2)F_1] \}$$

$$+ \tfrac{7}{6}\eta^2 F_1 \{ \exp(-\tilde{\kappa}(\vec{z}'^*)^2/2)(\vec{z}'^* \cdot \hat{\omega}')(\vec{z} \cdot \hat{\omega}')[1 + \tfrac{7}{6}(1 - \eta)(\vec{z}'^* \cdot \hat{\omega})^2]$$

$$+ \exp(-\tilde{\kappa}\vec{z}^2/2)(\vec{z}'^* \cdot \hat{\omega})(\vec{z} \cdot \hat{\omega})[1 + \tfrac{7}{6}(1 - \eta)(\vec{z} \cdot \hat{\omega}')^2] \} .$$

2. $({}^3\text{H} + \alpha) + [n + {}^6\text{Li}(20)]$ coupling kernels

The normalization kernel is

$$\langle \Phi^{\vec{z}'}({}^3\text{H} + \alpha) \mid \Phi^{\vec{z},\hat{\omega}}(n + {}^6\text{Li}) \rangle = -\tfrac{7}{12}(\tfrac{3}{2})^{1/2}(\vec{z}'^* \cdot \hat{\omega})^2 \left[\exp\left[\frac{\sqrt{2}}{3} \vec{z}'^* \cdot \vec{z} \right] - \exp\left[-\frac{\sqrt{2}}{4} \vec{z}'^* \cdot \vec{z} \right] \right] .$$

The kinetic energy kernel is

$$\langle \Phi^{\vec{z}'}(^3H+\alpha) \mid \sum_{i=1}^{7} T_i - T_{c.m.} \mid \Phi^{\vec{z},\hat{\omega}}(n+^6Li)\rangle$$

$$= -\tfrac{7}{12}(\tfrac{3}{2})^{1/2}E_u(\vec{z}'^*\cdot\hat{\omega})^2 \left\{ \exp\left[\frac{\sqrt{2}}{3}\vec{z}'^*\cdot\vec{z}\right]\left[\tfrac{22}{3}-\tfrac{1}{3}((\vec{z}'^*)^2+\vec{z}^2)+\frac{2\sqrt{2}}{9}\vec{z}'^*\cdot\vec{z}\right]\right.$$

$$\left. - \exp\left[-\frac{\sqrt{2}}{4}\vec{z}'^*\cdot\vec{z}\right]\left[\tfrac{22}{3}-\tfrac{1}{3}((\vec{z}'^*)^2+\vec{z}^2)-\frac{\sqrt{2}}{6}\vec{z}'^*\cdot\vec{z}\right]\right\}.$$

The interaction kernel is

$$\langle \Phi^{\vec{z}'}(^3H+\alpha)\mid \sum_{i<j}^{7} V_{ij}\mid \Phi^{\vec{z},\hat{\omega}}(n+^6Li)\rangle = -(\tfrac{3}{2})^{1/2}\widetilde{V}_0\left[\exp\left[\frac{\sqrt{2}}{3}\vec{z}'^*\cdot\vec{z}\right]G^{(d)} - \exp\left[-\frac{\sqrt{2}}{4}\vec{z}'^*\cdot\vec{z}\right]G^{(e)}\right],$$

where

$$G^{(d)}=\tfrac{7}{12}(\vec{z}'^*\cdot\hat{\omega})^2(X_d+X_e+F_1)+2\eta F_1$$

$$+\exp(-\widetilde{\kappa}'(\vec{z}'^*)^2/2)\{\tfrac{7}{12}(\vec{z}'^*\cdot\hat{\omega})^2[(1-\eta)X_d+\eta X_e-2\eta(1-\eta)F_1]-2\eta F_1\}$$

$$+\exp(-\widetilde{\kappa}\vec{z}^2/2)\left[\tfrac{7}{12}(\vec{z}'^*\cdot\hat{\omega})^2+\frac{7}{6\sqrt{2}}\eta(\vec{z}'^*\cdot\hat{\omega})(\vec{z}\cdot\hat{\omega})\right][\tfrac{1}{2}(X_d+X_e)-F_1]$$

$$+\exp(-\widetilde{\kappa}'(\vec{z}'^*)^2/2-\widetilde{\kappa}\vec{z}^2/2-(\widetilde{\kappa}'\widetilde{\kappa})^{1/2}\vec{z}'^*\cdot\vec{z})$$

$$\times\left[\tfrac{7}{12}(\vec{z}'^*\cdot\hat{\omega})^2\{\tfrac{1}{2}X_d-\eta[\tfrac{1}{2}(X_d+X_e)-F_1]\}-\frac{7}{6\sqrt{2}}(\vec{z}'^*\cdot\hat{\omega})(\vec{z}\cdot\hat{\omega})\eta[\tfrac{1}{2}(X_d+X_e)-F_1]\right],$$

$$G^{(e)}=\tfrac{7}{12}(\vec{z}'^*\cdot\hat{\omega})^2(X_d+X_e)+2\eta F_1+\exp(-\widetilde{\kappa}'(\vec{z}'^*)^2/2)\{\tfrac{7}{12}(\vec{z}'^*\cdot\hat{\omega})^2[(1-\eta)X_d+\eta X_e+(1-2\eta+2\eta^2)F_1]-2\eta F_1\}$$

$$+\exp(-\widetilde{\kappa}\vec{z}^2/2)\left\{\tfrac{7}{24}(\vec{z}'^*\cdot\hat{\omega})^2(X_d+X_e)-\frac{7}{6\sqrt{2}}\eta(\vec{z}'^*\cdot\hat{\omega})(\vec{z}\cdot\hat{\omega})[\tfrac{1}{2}(X_d+X_e)-F_1]\right\}$$

$$+\exp(-\widetilde{\kappa}'(\vec{z}'^*)^2/2-\widetilde{\kappa}\vec{z}^2/2+(\widetilde{\kappa}'\widetilde{\kappa})^{1/2}\vec{z}'^*\cdot\vec{z})$$

$$\times\left[\tfrac{7}{12}(\vec{z}'^*\cdot\hat{\omega})^2\{-\tfrac{1}{2}X_e+(1-\eta)[\tfrac{1}{2}(X_d+X_e)-F_1]\}+\frac{7}{6\sqrt{2}}\eta(\vec{z}'^*\cdot\hat{\omega})(\vec{z}\cdot\hat{\omega})[\tfrac{1}{2}(X_d+X_e)-F_1]\right].$$

APPENDIX B: NEW CALCULATIONAL METHOD OF RGM MATRIX ELEMENTS WITH GAUSSIAN BASIS FUNCTIONS

In this appendix, we describe a new method to calculate RGM matrix elements with Gaussian basis functions, starting from GCM kernels directly. Although we consider here the simplest case for clarity in presentation, it should be emphasized that this method is suitable for more complicated RGM kernels such as the coupling kernels shown in Appendix A and the three-cluster kernels to be discussed in a planned future publication.[27]

Consider a particular term of the GCM kernel for an operator $\mathcal{O}$, which has the form

$$I(\vec{z}'^*;\vec{z})=\langle A_\gamma(\vec{R},\vec{z}')\phi \mid \mathcal{O}P \mid A_\gamma(\vec{R},\vec{z})\phi\rangle$$

$$=\exp\{-\tfrac{1}{2}\rho(\vec{z}'^*)^2-\tfrac{1}{2}\sigma\vec{z}^2+\tau\vec{z}'^*\cdot\vec{z}\}. \quad \text{(B1)}$$

In the above equation, ϕ is a product of internal wave functions, P represents a certain permutation term, and the coefficients ρ, σ, and τ are determined by the interaction type and the number of nucleons interchanged between the clusters.[5,25] As is now well known, the RGM kernel $m(\vec{r}';\vec{r})$ corresponding to this term is obtained by the so-called Bargmann transformation which connects the Bargmann space (the Hilbert space of complex GCM) with the real space.[28-30] Namely, one finds

$$m(\vec{r}';\vec{r})=\langle \delta(\vec{R}-\vec{r}')\phi \mid \mathcal{O}P \mid \delta(\vec{R}-\vec{r})\phi\rangle$$

$$=\int d\mu(\vec{z}')d\mu(\vec{z})A_\gamma(\vec{r}',\vec{z}')A_\gamma(\vec{r},\vec{z})^*$$

$$\times I(\vec{z}'^*;\vec{z}), \quad \text{(B2)}$$

where $d\mu(\vec{z})$ is the three-dimensional Bargmann measure[28] defined by

$$d\mu(\vec{z})=\pi^{-3}\exp(-\vec{z}^*\cdot\vec{z})d^3(\text{Re}\vec{z})d^3(\text{Im}\vec{z}). \quad \text{(B3)}$$

We wish to calculate the matrix element

$$M_l(\lambda_1;\lambda_2) \equiv \langle \chi_{lm}(\vec{R},\lambda_1)\phi \mid \mathcal{O}P \mid \chi_{lm}(\vec{R},\lambda_2)\phi \rangle$$

$$= \int d\vec{r}'d\vec{r}\chi_{lm}(\vec{r}',\lambda_1)^*\chi_{lm}(\vec{r},\lambda_2)m(\vec{r}';\vec{r}) ,$$

where   (B4)

$$\chi_{lm}(\vec{r},\lambda) = \left[\frac{2^{2(l+1)}l!(2\lambda)^{l+3/2}}{(2l+1)!\sqrt{\pi}}\right]^{1/2} r^l e^{-\lambda r^2} Y_{lm}(\hat{r})$$

(B5)

is a Gaussian function with a width parameter λ. The Gaussian integral of Eq. (B4) is, of course, straightforward to evaluate, if we use the well-known formula[25]

$$m(\vec{r}';\vec{r}) = \left[\frac{2\gamma}{\pi}\frac{1}{D}\right]^{3/2}$$

$$\times \exp\left[-\left[2\frac{1-\sigma}{D}-1\right]\gamma\vec{r}'^2\right.$$

$$\left. -\left[2\frac{1-\rho}{D}-1\right]\gamma\vec{r}^2 + 4\frac{\tau}{D}\gamma\vec{r}'\cdot\vec{r}\right]$$

(B6)

with $D = (1-\rho)(1-\sigma)-\tau^2$. Instead of using this standard procedure, however, we propose here to use the following method which is even more convenient.

Suppose $I(\vec{z})$ is a GCM function of Gaussian form in the Bargmann space and $m(\vec{r})$ is the corresponding RGM function for $I(\vec{z})$; i.e.,

$$m(\vec{r}) = \int d\mu(\vec{z})A_\gamma(\vec{r},\vec{z})^*I(\vec{z}) .$$

(B7)

Then, we can easily prove that

$$M_{lm}(\lambda) \equiv \int d\vec{r}\chi_{lm}(\vec{r},\lambda)m(\vec{r})$$

$$= \left[\frac{\pi}{2\gamma}\right]^{3/4}\left[\frac{(2l+1)!!}{4\pi}(1-\epsilon^2)^{l+3/2}\right]^{1/2}$$

$$\times \left[\frac{1}{\sqrt{-\epsilon}}\right]^l\lim_{r\to 0}\left[\frac{1}{2\sqrt{\gamma}r}\right]^l\int d^2\hat{r}\,Y_{lm}(\hat{r})\tilde{m}(\vec{r}) ,$$

(B8)

where

$$\tilde{m}(\vec{r}) = \int d\mu(\vec{z})A_\gamma(\vec{r},\vec{z})^*I(\sqrt{-\epsilon}\vec{z})$$

(B9)

and

$$\epsilon = \frac{\gamma-\lambda}{\gamma+\lambda}$$

with

$$\sqrt{-\epsilon} = \begin{cases} -i\sqrt{\epsilon}, & 1 > \epsilon \geq 0 \\ \sqrt{|\epsilon|}, & 0 > \epsilon > -1 . \end{cases}$$

This formula is valid as long as the Gaussian integral in Eq. (B8) is absolutely convergent.

If the limit formula (B8) is used twice in Eq. (B4), it is easy to see that, to obtain $M_l(\lambda_1;\lambda_2)$, one merely needs to make the following replacements:

$$\rho \to -\epsilon_1\rho ,$$

$$\sigma \to -\epsilon_2\sigma ,$$ (B10)

$$\tau \to [(-\epsilon_1)^{1/2}]^*(-\epsilon_2)^{1/2}\tau ,$$

with

$$\epsilon_i \equiv \frac{\gamma-\lambda_i}{\gamma+\lambda_i} \quad (i=1,2)$$ (B11)

in the expression obtained by using $m(\vec{r}';\vec{r})$ of Eq. (B6) instead of $\tilde{m}(\vec{r})$ as in Eq. (B8). The final result is

$$M_l(\lambda_1;\lambda_2) = [(1-\epsilon_1^2)(1-\epsilon_2^2)]^{(l+3/2)/2}\left[\frac{1}{\widetilde{D}}\right]^{3/2}\left[\frac{\tau}{\widetilde{D}}\right]^l ,$$

(B12)

with

$$\widetilde{D} = (1+\epsilon_1\rho)(1+\epsilon_2\sigma)-\epsilon_1\epsilon_2\tau^2 .$$ (B13)

The matrix elements for the kinetic energy kernel can also be easily obtained in a similar way.

APPENDIX C: MATRIX ELEMENTS OF RGM COUPLING KERNELS

In this appendix, we give explicit expressions of RGM coupling matrix elements with Gaussian basis functions, obtained by applying the method described in Appendix B. In this particular case, it is necessary to classify each term of the GCM coupling kernels not only by the interaction type and the number of interchanged nucleons, but also by a number of different angular momentum types.

Suppose that one term of the GCM kernel for the $n + {}^6\text{Li}(20)$ system has the form

$$I^f(\vec{z}'^*,\hat{\omega}';\vec{z},\hat{\omega}) = I(\vec{z}'^*;\vec{z})f(\vec{z}'^*,\hat{\omega}',\vec{z},\hat{\omega}) ,$$ (C1)

where $I(\vec{z}'^*;\vec{z})$ is given by Eq. (B1) and $f(\vec{z}'^*,\hat{\omega}',\vec{z},\hat{\omega})$ represents various polynomials composed of the inner products of $\vec{z}'^*$, $\hat{\omega}'$, $\vec{z}$, and $\hat{\omega}$. The angular momentum projected matrix elements for $I^f(\vec{z}'^*,\hat{\omega}',\vec{z},\hat{\omega})$ with Gaussian basis functions can be written as

$$M_{ij}^f(\lambda_1;\lambda_2) = [(1-\epsilon_1^2)^{l_i+3/2}(1-\epsilon_2^2)^{l_j+3/2}]^{1/2}$$

$$\times \left[\frac{1}{\widetilde{D}}\right]^{3/2}\widetilde{M}_{ij}[f] ,$$ (C2)

where the index $i \equiv (l_i,I_i)L$ specifies a channel, and ϵ_1, ϵ_2, and $\widetilde{D}$ are given in Eqs. (B11) and (B13). For the $({}^3\text{H}+\alpha)+[n+{}^6\text{Li}(20)]$ GCM coupling kernels, we similarly write their matrix elements as

$$M_j^f(\lambda_1;\lambda_2) = [(1-\epsilon_1^2)^{L+3/2}(1-\epsilon_2^2)^{l_j+3/2}]^{1/2}$$

$$\times \left[\frac{1}{\widetilde{D}}\right]^{3/2}\widetilde{M}_j[f] ,$$ (C3)

where we now take $\epsilon_1 = (\gamma'-\lambda_1)/(\gamma'+\lambda_1)$.

The angular momentum types, which show up in both normalization and interaction kernels, are listed below in the normalization-kernel case by assuming an arbitrary choice of ρ, σ, and τ. As an angular momentum function in the $n + {}^6\text{Li}(20)$ coupled-channel problem, we introduce

$$G_{ij}^L(P_1, \ldots, P_6) \equiv \left[\frac{(2P_1+1)\hat{I}_i\hat{I}_j}{(4\pi)^2 A_{2I_i}A_{2I_j}}\right] \int d^2\hat{r}'d^2\hat{r}\,d^2\hat{\omega}'d^2\hat{\omega}[Y_{I_j}(\hat{r}')Y_{I_i}(\hat{\omega}')]^*_{LM}$$

$$\times [Y_{I_j}(\hat{r})Y_{I_j}(\hat{\omega})]_{LM} P_{P_1}(\hat{r}'\cdot\hat{r})P_{P_2}(\hat{r}'\cdot\hat{\omega})P_{P_3}(\hat{r}\cdot\hat{\omega}')P_{P_4}(\hat{\omega}'\cdot\hat{\omega})P_{P_5}(\hat{r}'\cdot\hat{\omega}')P_{P_6}(\hat{r}\cdot\hat{\omega})$$

$$= \left[\frac{(2P_1+1)\hat{I}_i\hat{I}_j}{A_{2I_i}A_{2I_j}}\right] \sum_{STS'T'} (-1)^{l_i+l_j+T+T'}\hat{S}\hat{T}\hat{S}'\hat{T}'$$

$$\times C(P_1P_2S)C(P_3P_4T)C(P_1P_3S')C(P_2P_4T')$$

$$\times C(P_5Sl_i)C(P_6S'l_j)C(P_5TI_i)C(P_6T'I_j)$$

$$\times \begin{Bmatrix} S & l_i & P_5 \\ I_i & T & L \end{Bmatrix}\begin{Bmatrix} S' & l_j & P_6 \\ I_j & T' & L \end{Bmatrix}\begin{Bmatrix} P_1 & P_2 & S \\ P_3 & P_4 & T \\ S' & T' & L \end{Bmatrix} \tag{C4}$$

with $\hat{a} = (2a+1)^{1/2}$, $C(abc) = \langle a0b0|c0\rangle$, and A_{2I} given by Eq. (A2). For the $(^3H + \alpha) + [n + {}^6Li(20)]$ case, we define the quantities

$$H_1^L = \left[\frac{(L+1)(L+2)(2L+5)}{(2L+1)}\right]^{1/2},$$

$$H_2^L(I=0) = \frac{2L}{\sqrt{3}}, \tag{C5}$$

$$H_2^L(I=2) = \left[\frac{2L(L+1)(2L+3)}{3(2L-1)}\right]^{1/2}.$$

Also, we use the following notation to make the expressions compact:

$$\tilde{\tau} = \frac{\tau}{\tilde{D}}, \quad \tilde{\rho} = \frac{1+\epsilon_1\rho}{\tilde{D}}, \quad \tilde{\sigma} = \frac{1+\epsilon_2\sigma}{\tilde{D}}, \quad Q = \frac{1-\epsilon_1-\epsilon_2+\epsilon_1\epsilon_2\tau^2}{\tilde{D}}. \tag{C6}$$

1. n + ^{6}Li(20) matrix elements

The normalization kernel is

$$\tilde{M}_{ij}[(\hat{\omega}'\cdot\hat{\omega})^2] = \delta_{ij}\tilde{\tau}^{l_i},$$

$$\tilde{M}_{ij}[(\hat{\omega}'\cdot\hat{\omega})(\vec{z}'^*\cdot\hat{\omega})(\vec{z}\cdot\hat{\omega}')] = \delta_{ij}\epsilon_1\epsilon_2\tilde{\tau}^{l_i+1} + \delta_{l_il_j}(2l_i+1)\tilde{\tau}^{l_i-1}[\tilde{\rho}\tilde{\sigma}G_{ij}^L(l_i-111100) + \epsilon_1\epsilon_2\tilde{\tau}^2 G_{ij}^L(l_i-100111)]$$

$$+ \delta_{l_i-2,l_j}[(2l_i+1)(2l_i-1)]^{1/2}\epsilon_2\tilde{\tau}^{l_j+1}\tilde{\sigma}G_{ij}^L(l_j10110)$$

$$+ \delta_{l_i,l_j-2}[(2l_j+1)(2l_j-1)]^{1/2}\epsilon_1\tilde{\tau}^{l_i+1}\tilde{\rho}G_{ij}^L(l_i01101).$$

The kinetic energy kernel is ($\rho = \sigma = 0$ only)

$$\tilde{M}_{ij}\{(\hat{\omega}'\cdot\hat{\omega})^2[1-\tfrac{1}{3}((\vec{z}'^*)^2+\vec{z}^2)+\tfrac{2}{3}\tau\vec{z}'^*\cdot\vec{z}]\} = \delta_{ij}\tilde{\tau}^{l_i}(1+\tfrac{2}{3}l_i)Q,$$

$$\tilde{M}_{ij}\{(\hat{\omega}'\cdot\hat{\omega})(\vec{z}'^*\cdot\hat{\omega})(\vec{z}\cdot\hat{\omega}')[\tfrac{5}{3}-\tfrac{1}{3}((\vec{z}'^*)^2+\vec{z}^2)+\tfrac{2}{3}\tau\vec{z}'^*\cdot\vec{z}]\}$$

$$= \tfrac{2}{3}\delta_{ij}\epsilon_1\epsilon_2\tilde{\tau}^{l_i+1}[1+(l_i+\tfrac{5}{2})Q] + \tfrac{2}{3}\delta_{l_il_j}(2l_i+1)\tilde{\tau}^{l_i-1}\left\{\left[\frac{1}{\tilde{D}}\right]^2[\epsilon_1+\epsilon_2-1+(l_i+\tfrac{5}{2})Q]G_{ij}^L(l_i-111100)\right.$$

$$\left.+ \epsilon_1\epsilon_2\tilde{\tau}^2[1+(l_i+\tfrac{5}{2})Q]G_{ij}^L(l_i-100111)\right\}$$

$$+ \tfrac{2}{3}\delta_{l_i-2,l_j}[(2l_i+1)(2l_i-1)]^{1/2}\epsilon_2\tilde{\tau}^{l_j+1}\frac{1}{\tilde{D}}[\epsilon_2+(l_j+\tfrac{7}{2})Q]G_{ij}^L(l_j10110)$$

$$+ \tfrac{2}{3}\delta_{l_i,l_j-2}[(2l_j+1)(2l_j-1)]^{1/2}\epsilon_1\tilde{\tau}^{l_i+1}\frac{1}{\tilde{D}}[\epsilon_1+(l_i+\tfrac{7}{2})Q]G_{ij}^L(l_i01101).$$

The interaction kernel is

$$\widetilde{M}_{ij}[1]=\delta_{ij}\delta_{I_i,0}3\widetilde{\tau}^{l_i} \ ,$$

$$\widetilde{M}_{ij}[(\widehat{\omega}'\cdot\widehat{\omega})(\vec{z}'^*\cdot\widehat{\omega}')(\vec{z}\cdot\widehat{\omega})]$$

$$=\delta_{ij}\epsilon_1\epsilon_2\widetilde{\tau}^{l_i+1}+\delta_{l_il_j}(2l_i+1)\widetilde{\tau}^{l_i-1}[\widetilde{\rho\sigma}G_{ij}^L(l_i-100111)+\epsilon_1\epsilon_2\widetilde{\tau}^2G_{ij}^L(l_i-111100)]$$

$$+\delta_{l_i-2,l_j}[(2l_i+1)(2l_i-1)]^{1/2}\epsilon_2\widetilde{\tau}^{l_j+1}\widetilde{\sigma}G_{ij}^L(l_j10110)+\delta_{l_i,l_j-2}[(2l_j+1)(2l_j-1)]^{1/2}\epsilon_1\widetilde{\tau}^{l_i+1}\widetilde{\rho}G_{ij}^L(l_i01101) \ ,$$

$$\widetilde{M}_{ij}[(\widehat{\omega}'\cdot\widehat{\omega})(\vec{z}'^*\cdot\widehat{\omega}')(\vec{z}'^*\cdot\widehat{\omega})]$$

$$=\delta_{ij}\epsilon_1\widetilde{\tau}^{l_i}\widetilde{\sigma}+\delta_{l_il_j}(2l_i+1)\epsilon_1\widetilde{\tau}^{l_i}\widetilde{\sigma}[G_{ij}^L(l_i-100111)+G_{ij}^L(l_i-111100)]$$

$$+\delta_{l_i-2,l_j}[(2l_i+1)(2l_i-1)]^{1/2}\widetilde{\tau}^{l_j}\widetilde{\sigma}^2G_{ij}^L(l_j10110)+\delta_{l_i,l_j-2}[(2l_j+1)(2l_j-1)]^{1/2}\epsilon_1^2\widetilde{\tau}^{l_i+2}G_{ij}^L(l_i01101) \ ,$$

$$\widetilde{M}_{ij}[(\vec{z}'^*\cdot\widehat{\omega}')(\vec{z}\cdot\widehat{\omega}')]$$

$$=3\delta_{ij}\delta_{I_i,0}\epsilon_1\epsilon_2\widetilde{\tau}^{l_i+1}+\delta_{l_il_j}(2l_i+1)\widetilde{\tau}^{l_i-1}(\widetilde{\rho\sigma}+\epsilon_1\epsilon_2\widetilde{\tau}^2)G_{ij}^L(l_i-101010)$$

$$+\tfrac{2}{3}\delta_{l_i-2,l_j}[(2l_i+1)(2l_i-1)]^{1/2}\epsilon_2\widetilde{\tau}^{l_j+1}\widetilde{\sigma}G_{ij}^L(l_j00020)+\tfrac{2}{3}\delta_{l_i,l_j-2}[(2l_j+1)(2l_j-1)]^{1/2}\epsilon_1\widetilde{\tau}^{l_i+1}\widetilde{\rho}G_{ij}^L(l_i02000) \ .$$

$$\widetilde{M}_{ij}[(\vec{z}'^*\cdot\widehat{\omega}')(\vec{z}\cdot\widehat{\omega}')(\vec{z}'^*\cdot\widehat{\omega})^2]$$

$$=\delta_{ij}\epsilon_1^2\epsilon_2\widetilde{\tau}^{l_i+1}\widetilde{\sigma}(3\delta_{I_i,0}+2)$$

$$+\delta_{l_il_j}(2l_i+1)\epsilon_1\widetilde{\sigma}\{\widetilde{\tau}^{l_i-1}(\widetilde{\rho\sigma}+\epsilon_1\epsilon_2\widetilde{\tau}^2)[2G_{ij}^L(l_i-111100)+G_{ij}^L(l_i-101010)]$$

$$+2\epsilon_1\epsilon_2\widetilde{\tau}^{l_i+1}[2G_{ij}^L(l_i-100111)+G_{ij}^L(l_i-110001)]\}$$

$$+\delta_{l_i-2,l_j}[(2l_i+1)(2l_i-1)]^{1/2}\epsilon_2\widetilde{\tau}^{l_j+1}\widetilde{\sigma}^2\{4G_{ij}^L(l_j10110)+\tfrac{2}{3}[G_{ij}^L(l_j00020)+G_{ij}^L(l_j20000)]\}$$

$$+\delta_{l_i,l_j-2}[(2l_j+1)(2l_j-1)]^{1/2}\epsilon_1^2\widetilde{\tau}^{l_i+1}\{2(\widetilde{\rho\sigma}+\epsilon_1\epsilon_2\widetilde{\tau}^2)G_{ij}^L(l_i01101)+\tfrac{2}{3}[\widetilde{\rho\sigma}G_{ij}^L(l_i02000)+\epsilon_1\epsilon_2\widetilde{\tau}^2G_{ij}^L(l_i00002)]\}$$

$$+\delta_{l_il_j}(2l_i+1)(2l_i-1)\epsilon_1\widetilde{\tau}^{l_i-1}\widetilde{\sigma}\{2(\widetilde{\rho\sigma}+\epsilon_1\epsilon_2\widetilde{\tau}^2)G_{ij}^L(l_i-211011)$$

$$+\tfrac{4}{9}[\widetilde{\rho\sigma}G_{ij}^L(l_i-222000)+\epsilon_1\epsilon_2\widetilde{\tau}^2G_{ij}^L(l_i-200022)]\}$$

$$+\delta_{l_i-2,l_j}(2l_j+1)[(2l_i+1)(2l_i-1)]^{1/2}\widetilde{\tau}^{l_j-1}\widetilde{\sigma}^2[\tfrac{2}{3}(\widetilde{\rho\sigma}+\epsilon_1\epsilon_2\widetilde{\tau}^2)G_{ij}^L(l_j-121010)+\tfrac{4}{3}\epsilon_1\epsilon_2\widetilde{\tau}^2G_{ij}^L(l_j-110021)]$$

$$+\delta_{l_i,l_j-2}(2l_i+1)[(2l_j+1)(2l_j-1)]^{1/2}\epsilon_1^2\widetilde{\tau}^{l_i+1}[\tfrac{2}{3}(\widetilde{\rho\sigma}+\epsilon_1\epsilon_2\widetilde{\tau}^2)G_{ij}^L(l_i-101012)+\tfrac{4}{3}\widetilde{\rho\sigma}G_{ij}^L(l_i-112001)]$$

$$+\tfrac{4}{9}\delta_{l_i-4,l_j}[(2l_i+1)(2l_i-1)(2l_i-3)(2l_i-5)]^{1/2}\epsilon_2\widetilde{\tau}^{l_j+1}\widetilde{\sigma}^3G_{ij}^L(l_j20020)$$

$$+\tfrac{4}{9}\delta_{l_i,l_j-4}[(2l_j+1)(2l_j-1)(2l_j-3)(2l_j-5)]^{1/2}\epsilon_1^3\widetilde{\tau}^{l_i+3}\widetilde{\rho}G_{ij}^L(l_i02002) \ .$$

2. $(^3H+\alpha)+[n+^6Li(20)]$ coupling matrix elements

The normalization kernel is

$$\widetilde{M}_j[(\vec{z}'^*\cdot\widehat{\omega})^2]=\widetilde{\tau}^{l_j}[-\delta_{L,l_j}\epsilon_1\widetilde{\sigma}(\sqrt{3}\delta_{I_j,0}+H_2^L(I_j))+\delta_{I_j,2}\{\delta_{L-2,l_j}[(l_j+1)(l_j+2)]^{1/2}\widetilde{\sigma}^2+\delta_{L,l_j-2}\epsilon_1^2H_1^L\}] \ .$$

The kinetic energy kernel is $(\rho=\sigma=0$ only$)$

$$\widetilde{M}_j\{(\vec{z}'^*\cdot\widehat{\omega})^2[\tfrac{22}{3}-\tfrac{1}{3}((\vec{z}'^*)^2+\vec{z}^2)+\tfrac{2}{3}\tau\vec{z}'^*\cdot\vec{z}]\}$$

$$=\widetilde{\tau}^{l_j}\left\{-\delta_{L,l_j}\epsilon_1\frac{1}{\widetilde{D}}[\sqrt{3}\delta_{I_j,0}+H_2^L(I_j)][\tfrac{17}{3}+\tfrac{2}{3}\epsilon_2+\tfrac{2}{3}(l_j+\tfrac{5}{2})Q]\right.$$

$$\left.+\delta_{L-2,l_j}\delta_{I_j,2}[(l_j+1)(l_j+2)]^{1/2}\left[\frac{1}{\widetilde{D}}\right]^2[5+\tfrac{4}{3}\epsilon_2+\tfrac{2}{3}(l_j+\tfrac{7}{2})Q]+\delta_{L,l_j-2}\delta_{I_j,2}\epsilon_1^2H_1^L[\tfrac{19}{3}+\tfrac{2}{3}(L+\tfrac{7}{2})Q]\right\} \ .$$

The interaction kernel is

$$\widetilde{M}_j[1] = -\sqrt{3}\,\delta_{L,l_j}\delta_{I_j,0}\widetilde{\tau}^L \ ,$$

$$\widetilde{M}_j[(\widetilde{\mathbf{z}}'^*\cdot\hat{\omega})(\widetilde{\mathbf{z}}\cdot\hat{\omega})] = -\delta_{L,l_j}[\sqrt{3}\,\delta_{I_j,0}\epsilon_1\epsilon_2\widetilde{\tau}^{L+1} + \tfrac{1}{2}\widetilde{\tau}^{L-1}(\widetilde{\rho}\widetilde{\sigma} + \epsilon_1\epsilon_2\widetilde{\tau}^2)H_2^L(I_j)]$$

$$+ \delta_{I_j,2}\{\delta_{L-2,l_j}[(l_j+1)(l_j+2)]^{1/2}\epsilon_2\widetilde{\tau}^{l_j+1}\widetilde{\sigma} + \delta_{L,l_j-2}\epsilon_1\widetilde{\tau}^{L+1}\widetilde{\rho}H_1^L\} \ .$$

[1]J. A. Wheeler, Phys. Rev. 52, 1083 (1937); 52, 1107 (1937).

[2]K. Wildermuth and Y. C. Tang, A Unified Theory of the Nucleus (Vieweg, Braunschweig, Germany, 1977); Y. C. Tang, M. LeMere, and D. R. Thompson, Phys. Rep. 47, 167 (1978); K. Ikeda et al., Prog. Theor. Phys. Suppl. 68, 1 (1980).

[3]A. Arima, H. Horiuchi, K. Kubodera, and N. Takigawa, in Advances in Nuclear Physics, edited by M. Baranger and E. Vogt (Plenum, New York, 1972), Vol. 5, p. 345.

[4]Y. C. Tang, Microscopic Description of the Nuclear Cluster Theory, Vol. 145 of Lecture Notes in Physics (Springer, Berlin, 1981), and references contained therein.

[5]M. LeMere, D. J. Stubeda, H. Horiuchi, and Y. C. Tang, Nucl. Phys. A320, 449 (1979).

[6]J. N. Bahcall, W. F. Heubner, S. H. Lubow, P. D. Parker, and R. K. Ulrich, Rev. Mod. Phys. 54, 767 (1982).

[7]H. Walliser, Q. K. K. Liu, H. Kanada, and Y. C. Tang, Phys. Rev. C 28, 57 (1983).

[8]H. Kanada, T. Kaneko, and Y. C. Tang, Nucl. Phys. A380, 87 (1982).

[9]M. V. Mihailović and M. Poljšak, Nucl. Phys. A311, 377 (1978); R. Beck, R. Krivec, and M. V. Mihailović, ibid. A363, 365 (1981).

[10]H. Kanada, T. Kaneko, and Y. C. Tang, Nucl. Phys. A389, 285 (1982); D. R. Thompson and Y. C. Tang, Phys. Rev. C 8, 1649 (1973).

[11]D. R. Thompson, M. LeMere, and Y. C. Tang, Nucl. Phys. A286, 53 (1977).

[12]Y. Fujiwara and Y. C. Tang, Phys. Rev. C 27, 2457 (1983).

[13]In particular, the n + ^{6}Li*$(T=1)$ cluster configuration is expected to have a very small influence, since it has been experimentally found that the cross section for the ^{4}He(^{3}He,p) reaction leading to the first $T=1$ state of ^{6}Li at 3.56 MeV is very small [J. A. Koepke and R. E. Brown, Phys. Rev. C 16, 18 (1977)].

[14]M. Kamimura, Prog. Theor. Phys. Suppl. 62, 236 (1977).

[15]The indices of the S-matrix element have the following meaning. The superscript represents the total orbital angular momentum of the system. The subscript on the right side of the comma represents the relative orbital angular momentum

of the ^{3}H and α clusters in the incident channel, while the subscripts on the left side of the comma represent the orbital angular momentum values characterizing the exit channel which can be either the ^{3}H + α channel, or the n + ^{6}Li or n+^{6}Li* channel.

[16]F. Ajzenberg-Selove, Nucl. Phys. A320, 1 (1979).

[17]The cluster internal functions and the nucleon-nucleon potentials employed are somewhat different in these three calculations. These differences are, however, not expected to appreciably affect the contributions of specific distortion in the ^{3}H+α system.

[18]E. P. Wigner, Phys. Rev. 73, 1002 (1948); L. D. Landau and E. M. Lifshiftz, Quantum Mechanics, 3rd ed. (Pergamon, Oxford, England, 1977).

[19]The cusp behavior in the $L=0$, ^{3}He+α phase shift should be quite weak. The reason is that the ^{3}He+α configuration is not strongly coupled to the n+^{6}Be channel (see Ref. 13).

[20]R. D. Furber, R. E. Brown, G. L. Peterson, D. R. Thompson, and Y. C. Tang, Phys. Rev. C 25, 23 (1982).

[21]M. LeMere, Y. Fujiwara, Y. C. Tang, and Q. K. K. Liu, Phys. Rev C 26, 1847 (1982).

[22]Y. W. Lui, O. Karban, A. K. Basak, C. O. Blyth, J. M. Nelson, and S. Roman, Nucl. Phys. A297, 189 (1978).

[23]The RGM kernel of the ^{3}H + α system has already been derived by several authors [Y. C. Tang, E. Schmid, and K. Wildermuth, Phys. Rev. 131, 2631 (1963); K. Aoki and H. Horiuchi, Prog. Theor. Phys. 68, 2028 (1982)].

[24]For convenience in presenting the mathematical formulas, the notation used in the Appendices is slightly different from that used in the main text. However, the difference is quite minor and should not cause any confusion.

[25]H. Horiuchi, Prog. Theor. Phys. Suppl. 62, 90 (1977).

[26]It should be noted that $\phi_6(I=0)$ and $\phi_6^*(I=2)$ in Eqs. (3) and (4) are just the spatial parts of $\phi_{(20)IM}(^6$Li).

[27]Y. Fujiwara and Y. C. Tang, submitted to Nucl. Phys. A.

[28]V. Bargmann, Rev. Mod. Phys. 34, 829 (1962).

[29]T. H. Seligman and W. Zahn, J. Phys. G 2, 79 (1976).

[30]H. Horiuchi, Prog. Theor. Phys. 55, 1448 (1976).